

# Simulation of subseismic joint and fault networks using a heuristic mechanical model

PAUL GILLESPIE<sup>1\*</sup>, GIULIO CASINI<sup>1</sup>, HAYLEY IBEN<sup>2,3</sup> & JAMES F. O'BRIEN<sup>3</sup>

<sup>1</sup>*Statoil ASA, Forusbein 50, 4035 Stavanger, Norway*

<sup>2</sup>*Pixar Animation Studios, 1200 Park Ave., Emeryville, CA 94608, USA*

<sup>3</sup>*EECS, Computer Science Division, University of California, Berkeley, CA, USA*

\*Correspondence: pgil@statoil.com

**Abstract:** Flow simulations of fractured and faulted reservoirs require representation of subseismic structures about which subsurface data are limited. We describe a method for simulating fracture growth that is mechanically based but heuristic, allowing for realistic modelling of fracture networks with reasonable run times. The method takes a triangulated meshed surface as input, together with an initial stress field. Fractures initiate and grow based on the stress field, and the growing fractures relieve the stress in the mesh. We show that a wide range of bedding plane joint networks can be modelled simply by varying the distribution and anisotropy of the initial stress field. The results are in good qualitative agreement with natural joint patterns. We then apply the method to a set of parallel veins and demonstrate how the variations in thickness of the veins can be represented. Lastly, we apply the method to the simulation of normal fault patterns on salt domes. We derive the stress field on the bedding surface using the horizon curvature. The modelled fault network shows both radial and concentric faults. The new method provides an effective means of modelling joint and fault networks that can be imported to the flow simulator.

Subseismic fractures such as small faults and joints are important both in fractured reservoirs, in which fractures provide significant permeability, and in porous sandstone reservoirs, in which faults may form barriers or baffles to flow. In either case, the topology of the fracture network has a critical control on the dynamic behaviour of fluids in the reservoir. A typical approach to modelling fractured reservoirs is to use discrete fracture network models (DFNs) in which the individual fractures are placed independently according to a stochastic process (e.g. Barr *et al.* 2007; Rogers *et al.* 2007). Similarly, stochastic models are often used for representation of subseismic faults in sandstone reservoirs (e.g. Maerten *et al.* 2006). The stochastic methods can be highly effective, but have the drawback that there is no mechanical interaction between the fractures meaning that the fracture connectivity is not representative of a natural fracture system; the representation of connectivity is a well recognized problem in stochastic fracture networks (Odling & Webman 1991; Manzocchi 2002). An alternative is to create fracture networks using a geomechanical model, for instance using linear elastic fracture mechanics implemented in a boundary element model (e.g. Olson 1993; Renshaw & Pollard 1994; Tuckwell *et al.* 2003; Olson *et al.* 2007) or a finite discrete element model (FEMDEM) (e.g. Morris *et al.* 2006; Trivino & Mohanty 2015). The

difficulty with the geomechanical approach is that it is computationally expensive and simulation of the fractures at the scale of an oilfield is prohibitive. Furthermore, the required mechanical constants are usually poorly constrained under representative geological conditions.

In this article we present a method for modelling fractures which uses a heuristic mechanical model, that is, a model in which the stress field is only approximated and computation times are short, which allows realistic interaction between the fractures. The aim is to develop a technique that can readily produce plausible fracture simulations that can be taken further into the flow simulator. The mechanics are only approximate and the simulations are not suitable for detailed investigation of the process of fracturing. However, the method represents the stress interaction between the fractures in enough detail to allow for a good representation of the network topology.

## Mechanical model

We call the method the Surface Crack Simulator (SCS), which uses the algorithm first developed by Iben & O'Brien (2009), further developed by Iben (2007) and subsequently incorporated into in house software developed at Statoil. The method

uses the finite element technique and the input geometry is a triangulated surface, usually representing a horizon. An initial stress field is provided on the horizon by one of a variety of techniques and the fractures then grow in order to relieve that stress field. The fractures are Mode I, opening mode fractures. Rather than allowing the stress to equilibrate at each step of fracture growth, the stress is updated for a finite number of increments. This allows a stress shadow to develop around each fracture and stress concentration to build at the fracture tips. The fracture growth is controlled by a number of parameters including the material strength and relaxation rate that control the fracture nucleation and the size of the stress shadows around the fractures.

The Surface Crack Simulator models realistic fracture patterns on a generic surface using a first order quasi static system. The code assumes that all displacements of the simulated surface are small enough that, aside from crack formation, the geometry will remain fixed and the evolution of the stress field can be modelled directly. The code also assumes that movement and crack formation proceeds slowly enough that dynamic effects due to elastic waves can be ignored. These assumptions allow the use of a simplified quasistatic solver that is substantially faster and more stable than a second order dynamic simulation.

Fractures are generated on a triangle discretization of the input surface. The mesh may be planar or it may represent a surface in three dimensions (3D). Initial conditions are modelled by imposing a predetermined stress field over the triangle mesh. The stress field then evolves based on a process that models shrinkage, substrate movement or other effects. The stress field drives crack formation, which in turn relieves stress around the crack paths. The simulation has several input parameters that define the behaviour of the simulated surface material. Some of the parameters used by SCS are based on physical properties (e.g. failure strength of the material, relaxation) while others are heuristics (e.g. crack propagation factor, cracks per step).

### *Algorithm*

Once the initial stress values are assigned to the mesh, the stress field evolves through time by fracture generation (Iben & O'Brien 2009). Fractures appear and propagate through discrete cracking steps and local re meshing. After each cracking step the stress field is updated according to a relaxation process and the results are visualized. The process is repeated until the system reaches a stop criterion (i.e. there is a limit to the number of simulation steps or the fracture density).

In summary:

- (1) initialize the stress over the triangulated mesh;
- (2) compute failure criteria for each node and store in a priority queue;
- (3) crack the mesh at the node sitting at the top of the queue and perform local re meshing;
- (4) perform relaxation and update stress and queue;
- (5) post process the mesh to produce crack aperture; and
- (6) return to step (2) until stop criterion is reached.

### *Triangulated mesh*

The mesh used to represent a geological surface (such as bedding surface or interpreted top reservoir) is a triangulated mesh with randomized nodes and with fairly homogeneous triangle size. The code that creates the initial mesh avoids creating triangles with poor aspect ratios, as these can adversely affect the stability of the program. By using a triangulated mesh it is possible to represent complexly deformed surfaces such as deformed horizons associated with diapirs or recumbent folds.

### *Stress field*

The model requires an initial stress field which will be relieved by the growing cracks. The initial stress is stored as rank two tensors located in the centre of each triangle (Fig. 1a). The stress is assumed to be constant within a triangle. The stress tensor at each triangle is stored as a 2D quantity existing in the plane of the triangle. The stress tensor can be initialized in various ways, for instance it may be taken from an external geomechanical model such as a boundary element model. Here, following Iben & O'Brien (2009), we have applied two different methods for stress initialization: (1) uniform stress field; and (2) curvature generated stress.

In the simplest application, the triangulated mesh is assigned a uniform stress field which may be either isotropic ( $S_1 = S_2$ ) or anisotropic ( $S_1 > S_2$ ). The generation of stress using surface curvature is described in the section 'Simulation of Faults in Sea Domes'.

The Surface Crack Simulator stores the stress field as a piece wise constant rank two tensor field where values are stored at the barycentre of each triangle element (Fig. 1a). The stress field is interpolated to the node locations by computing the separation tensor at each node (O'Brien & Hodgins 1999) and using it as the stress at each node (Fig. 1c).

### *Compute failure criterion*

The net force acting on each node of the mesh is a vector in 3D space given by the sum of the forces

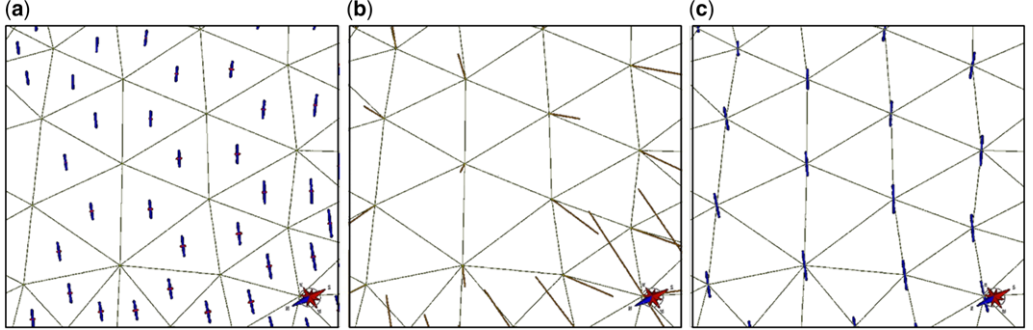


**Fig. 1.** Stress and failure criteria. (a) Stress tensors applied at the centre of each triangle of the mesh: blue ticks tensile, red ticks compressive. Length of ticks is proportional to stress magnitude. (b) Vertex forces at the nodes. (c) Separation tensors give estimates of the maximum principal tensile stress vectors at the nodes.

exerted by all surrounding triangles (Fig. 1b). The force exerted by an individual triangle lies in the plane of the triangle and depends on the area and geometry of the triangle and the stress tensor located in the centre of the triangle. An eigen decomposition is used at each node to compute the principal stresses at the node (Fig. 1c). If the magnitude of the largest tensile principal stress exceeds the assigned material strength (i.e. toughness), then a fracture will occur. The crack will lie in the plane perpendicular to the direction of the maximum tensile principal stress.

#### Generating cracks and re-meshing

For each iteration nodes are listed in a queue according to magnitude of largest value of  $\sigma_1$ , the maximum principal tensile stress. If this value is greater than material strength, a crack will occur

in the node with maximum value of  $\sigma_1$ . The crack develops along the fracture plane, defined as the plane perpendicular to the eigenvector associated with  $\sigma_1$  (Fig. 2). The triangles attached to the node at the tip of the fracture are split along the plane with the cracking node duplicated in order as to create, or extend, the mesh boundary. The triangles adjoining those that were split will also be split as required to maintain consistent triangulations.

Because the resolution of the triangle mesh is too coarse to represent fine scale effects that may cause initiated cracks to continue in a given direction once they start, SCS uses a heuristic called residual propagation to model this behaviour. When a crack is created in a mesh, the separation at the nodes representing the crack tip is modified by adding to them some amount of a tensor representing stress perpendicular to the fracture plane, that is, the separation tensor. The amount that is

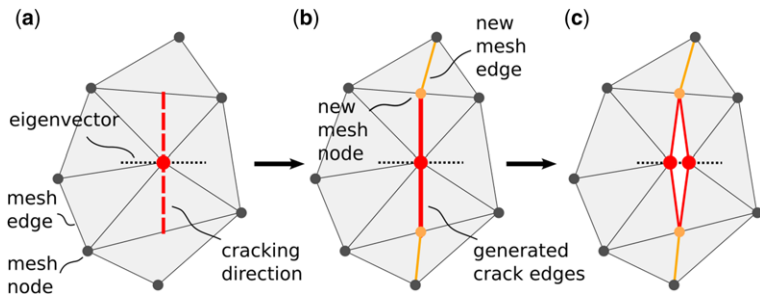


**Fig. 2.** Re-meshing at the crack position. (a) If the maximum eigenvalue of a node's separation tensor is above the strength threshold and at top of the queue, then the node (red node) is duplicated and the corresponding eigenvector representing  $\sigma_1$  (dotted black line) is used to compute the crack plane (dashed red line). (b) Where the crack plane (continuous red line) intersects the surrounding triangles, new nodes are generated (orange nodes) and a local re-meshing occurs to ensure that the surrounding elements are triangles (new mesh edges marked as continuous orange lines). (c) The duplicated nodes (red nodes) are separated along the eigenvector (dotted black line) to generate the aperture of the crack. From Iben (2007).

added is determined by a parameter  $\alpha$ , termed the crack propagation factor, which affects the straightness of the cracks.

### Stress update

The crack creates open boundaries in the mesh and reduces the perpendicular component of the nearby stress field according to elastic relaxation. The stress is assumed to be independent of deformation and relates to a first order relaxation process. Stress relaxation is treated as a diffusion process of rank two tensor quantities on a 3D mesh which redistributes stress from areas of high stress to areas of low stress. This diffusion is computed by using the sum of the forces acting on each node to compute a virtual displacement of the node, and then updating the stress in the surrounding elements based on these virtual displacements. The element stresses are then used to update the separation tensor at each node. For a more complete explanation of the relaxation process, see Iben (2007).

### Crack aperture

The sum of all forces exerted on a node along the fracture boundaries is determined and the crack aperture is calculated from the product of this sum and the number of iterations. This crack aperture has no mechanical effect on the simulation and is only used for visualization purposes.

### Iterations

The stress field is updated and, after eventual addition of incremental stress, the process can start a new iteration. The user is allowed to control the number of relaxation steps for each iteration and the relaxation rate.

### Model variables

The fracture development is controlled by a number of heuristic parameters:

- (1) toughness: approximately represents the fracture toughness of the material and controls the number of cracks;
- (2) crack propagation parameter: controls the smoothness of the crack trajectory and the length of the cracks;
- (3) relaxation step size: controls the width of the stress shadow;
- (4) relaxation steps: the number of steps in the relaxation process, controls the stress shadow width together with the relaxation step size;
- (5) iteration count ( $n$ ): the number of iterations; and
- (6) cracks per step: allows multiple cracks to be active during each step for faster simulation.

### Simulation of a single crack

The stress field developed around a single crack in the SCS is shown in Figure 3. Around the growing

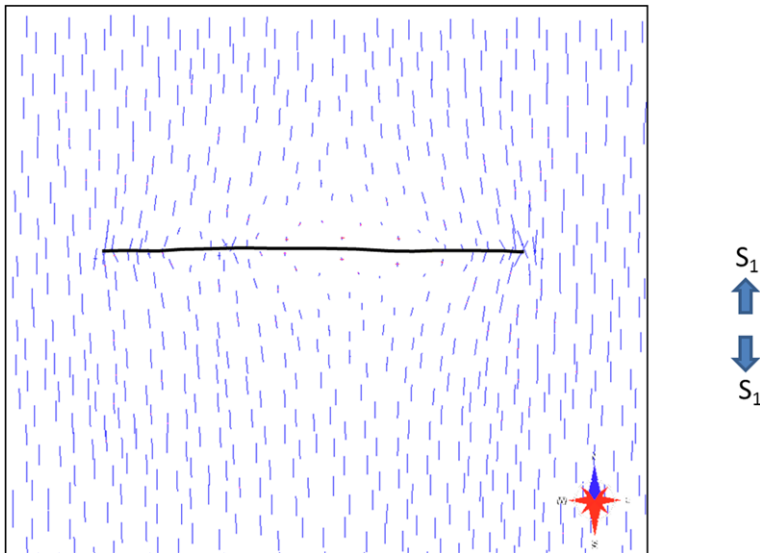


**Fig. 3.** Simulated stress field around an isolated crack propagated in the SCS model. Blue lines are the max tensile stress vectors. The surface was initialized with a uniform anisotropic tensile stress ( $S_2 = 0$ ).

crack there is a marked reduction in stress, or stress shadow, whereas there are stress concentrations close to the crack tips. The results are in qualitative agreement with results from linear elastic fracture mechanics (Pollard & Segall 1987).

## Simulation of joint patterns

### *Joint network growth*

We first apply the method to the simulation of joints. Joints are natural fractures formed in rocks that develop as Mode I cracks, formed under conditions of tensile stress or effective tensile stress (Pollard & Aydin 1988). The Surface Crack Simulator is therefore well suited to simulation of this kind of fracture (Iben 2007). Joints are often sub perpendicular to bedding and form a variety of patterns in the bedding plane, including parallel arrays, ladder patterns and polygonal patterns (Rives *et al.* 1994). In the latter two cases, the joints form very well connected networks characterized by 'T' shaped terminations.

Examples of joint patterns from the Jurassic of the Bristol Channel (Rawnsley *et al.* 1998; Bourne & Willemse 2001) are given in Figure 4. The connected joint system divides the rock into a series of blocks of characteristic size that is controlled by the thickness of the brittle unit. The first example (Fig. 4a) represents a ladder pattern with through going systematic joints connected by smaller cross joints, whereas the second example (Fig. 4b) represents a more irregular, polygonal pattern.

In order to simulate joint development we use a square planar triangulated mesh (Fig. 5) to represent the bedding plane, and initialize it with a uniform anisotropic tensile stress field with principal axes parallel to the boundaries of the mesh. The stress ratio, defined as  $R_S = S_2/S_1$ , was set to 0.5; other parameters are given in Table 1. The progressive development of the cracks (joints) is shown in Figure 6. At early stages, a single set of sub parallel joints develops. Subsequently, at around 3000 iterations, small connecting joints or cross joints develop spontaneously due to the relaxation of  $S_1$  and the swapping of the stress axes; this is known as the stress transition (Bai & Pollard 2000). With further iterations more cross joints appear, producing a series of equant blocks conforming to the ladder pattern. At high numbers of iterations the joint density does not increase significantly and the joint pattern is said to be saturated (Rives *et al.* 1992). The density of the fractures at saturation is determined in the model by the relaxation step size and the number of relaxation steps.

We then investigate the effect of the stress ratio  $R_S$  on the development of the joint patterns (Fig. 7).

At  $R_S = 0$  a single parallel set of joints develop. As there is no tensile stress parallel to the joints, cross joints do not develop even after large numbers of iterations. However, some of the joints curve towards each other at their terminations. At  $R_S = 0.25$ , some of the joints curve towards and terminate against other joints. In addition, cross joints are weakly developed.  $R_S = 0.5$  is the case already described in Figure 6 in which a ladder pattern is developed. At  $R_S = 0.75$  a ladder pattern is still developed, but the through going systematic joints are more irregular. Finally,  $R_S = 1$  represents isotropic stress, which causes an irregular, polygonal joint pattern to develop.

By simply modifying the stress ratio we are able to simulate a wide range of realistic joint patterns. The results compare well with fractured models developed using the boundary element technique combined with linear elastic fracture mechanics (Tuckwell *et al.* 2003; Olson *et al.* 2007) and are very similar to natural examples of joint patterns (Fig. 4).

### *Simulation of veins*

The joints described above do not have readily measurable apertures so the aperture was not visualized in the simulated results. However, in the case of mineral veins we can consider the thickness of the veins to represent the vein displacement, which can be simulated with SCS. An example (Fig. 8a) shows a single set of fibrous quartz/siderite veins from Millook Haven occurring in the overturned limb of a chevron fold (Jackson 1991; Johnston *et al.* 1994). The veins form a single sub parallel set and show relaying of vein displacement where vein tips are close and overlapping. The veins locally form en echelon arrays, implying a dextral shear sense.

A SCS simulation was made using parameters similar to parameters for the joint simulation (Fig. 8b) and using part of the same input mesh (dashed line Fig. 5). In order to create the single set of sub parallel fractures, the stress ratio  $R_S$  was set to 0.15. The crack propagation factor was reduced from 0.65 to 0.5 in order to create shorter fractures (Table 1). In this case the crack aperture was also included in the simulation.

The results show many of the characteristics of the vein map, including the lip shaped form of the veins and the formation of vein relays. The simulated veins are locally en echelon, although this pattern arises spontaneously without any asymmetry in the initial conditions (see also Olson & Pollard 1991). However, the strong en echelon pattern in the natural example is not reproduced as this is probably the result of local shear zones that are not represented in the model.

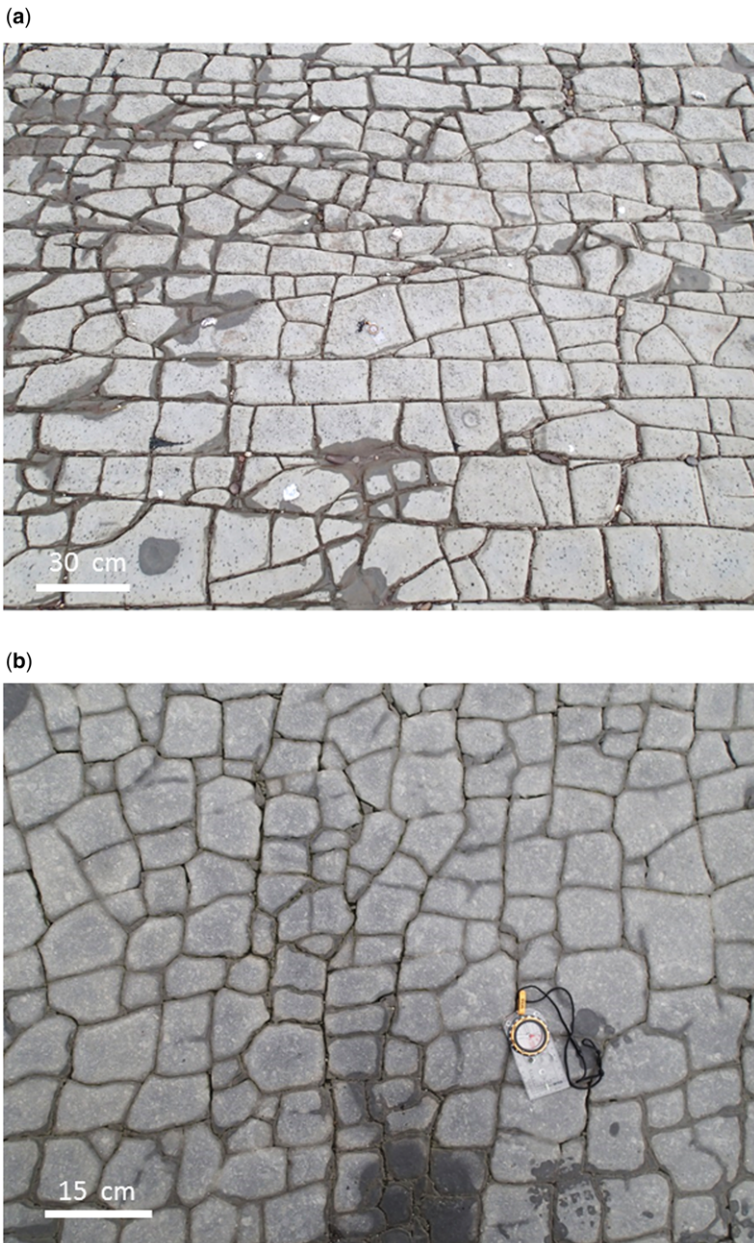


**Fig. 4.** (a) Bedding plane joint pattern from Lower Jurassic limestone of north Somerset at (a) Lilstock and (b) Blue Ben. In both examples the bedding planes are subhorizontal and the joints are subvertical and confined to the limestone unit.

### Application to normal faulting

The SCS was originally implemented for modelling the development of opening mode fractures such as joint traces in a surface. To what extent can it be applied to the problem of modelling normal faults

in a subhorizontal surface? In crack mechanics terms, the opening mode fracture is a Mode I crack and the normal fault is a Mode III crack. Analytical results from linear elastic fracture mechanics (Pollard & Segall 1987) allow us to compare the tensile stress perpendicular to a Mode I crack with the

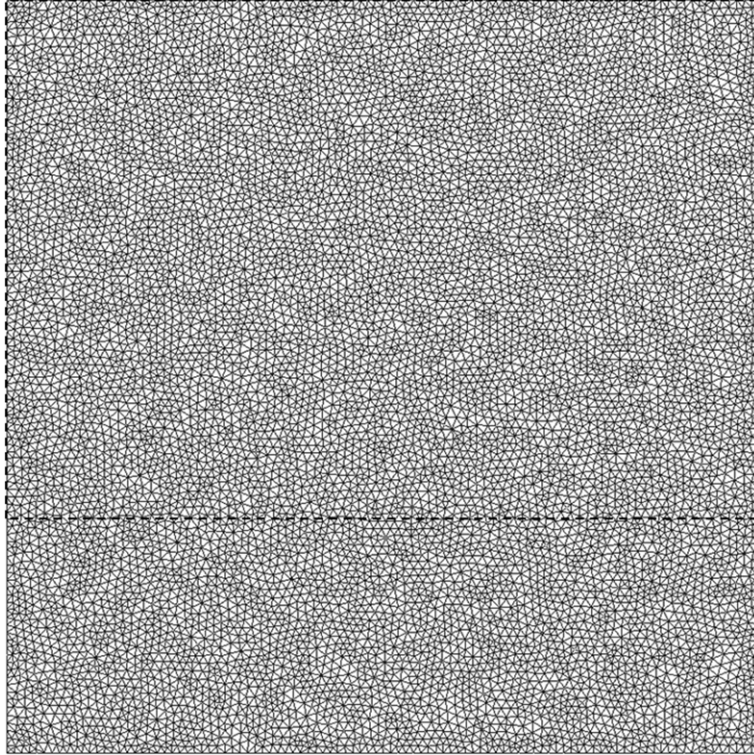


**Fig. 5.** Input mesh for joint pattern generation (Figs 6 & 7). Number of triangles = 19 290. Part of the mesh used for vein generation (Fig. 8) marked by dashed line.

crack parallel out of plane shear stress developed around a Mode III crack. Directly ahead of the crack tip, the stress magnitude is identical for the two modes of failure and so the propagation characteristics should be similar. However, in the direction perpendicular to the cracks, the stress perturbation is broader for the Mode I crack and narrower for the

Mode III crack. In the SCS model the width of the stress shadow is controlled heuristically rather than mechanically, so it is reasonable to simulate normal faults using SCS if the width of the stress shadow is suitably adjusted.

### Simulation of faults in salt domes

Salt domes represent a common phenomenon, and well described examples occur in Abu Dhabi, the onshore province of the Gulf Coast, USA, the Danish North Sea and the Barents Sea (Parker & McDowell 1955; Rank Friend & Elders 2004; Yamada *et al.* 2005; Mattos *et al.* 2016). Well developed salt domes are often cut by networks of faults that may provide fracture permeability or, in the case of sandstone reservoirs, may compartmentalize the reservoir (Fig. 9).

In order to simulate the fault pattern in salt domes we first generate a surface that represents the typical shape of a salt dome using elastic plate theory, initialize the stress in that surface using the principal curvatures, and then apply SCS using the surface cracks as a proxy for faults.

**Table 1.** Dimensionless parameters used in the Surface Crack Simulator to create the models for joints (Figs 6, 7), veins (Fig. 8) and the salt dome (Fig. 10)

Parameter	Model		
	Joint	Vein	Dome
Toughness	0.43	0.45	0.5
Crack propagation	0.65	0.5	0.9
Relaxation step size	0.002	0.002	0.015
No. relaxation steps	3	2	3
Iteration count	4500	2800	250
Cracks per step	1	1	1

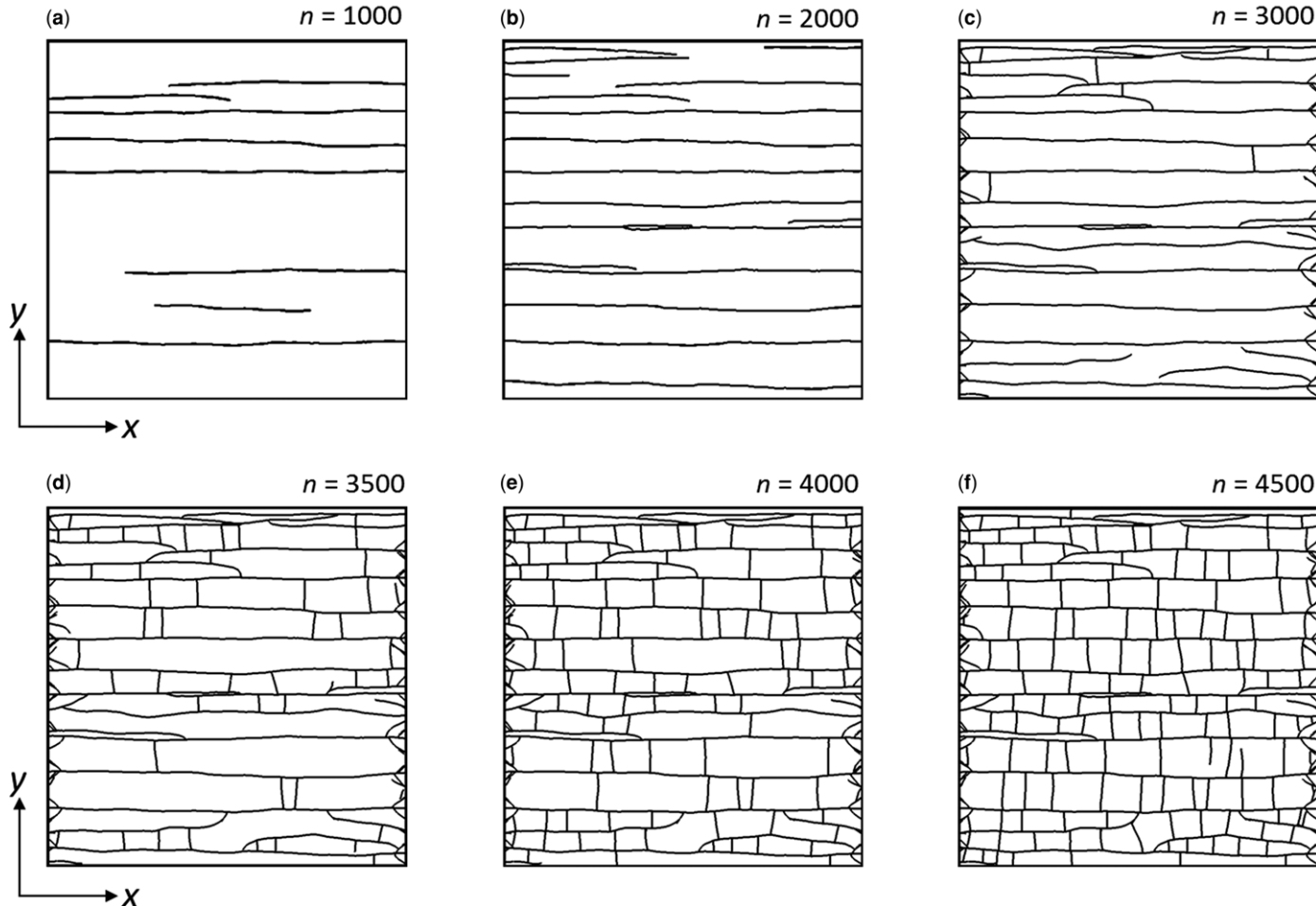


**Fig. 6.** (a–f) Simulation of cracks developing in an anisotropic stress field with stress ratio,  $R_S = 0.5$  and  $S_1$  parallel to  $y$  axis, shown in sequence at different numbers of iterations ( $n$ ). There is a boundary problem at the edge of the mesh which causes a locally increased crack density. This effect does not affect the results in the rest of the model.

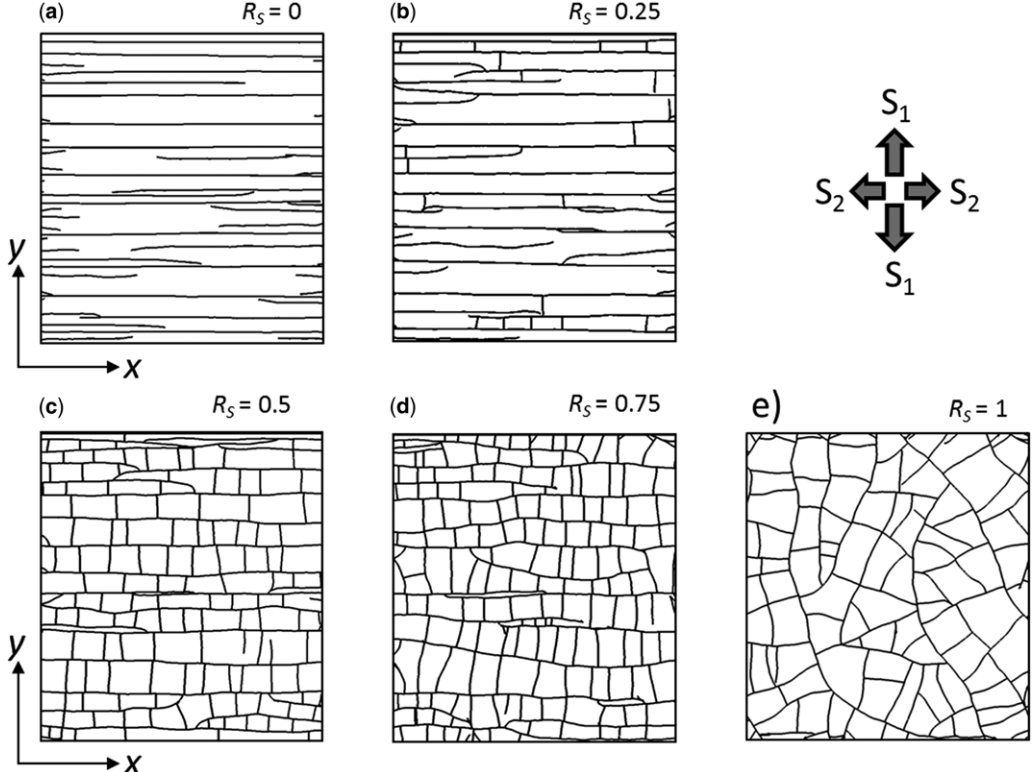


**Fig. 7.** Joint patterns simulated at different values of the stress ratio  $R_S$ . The number of iterations is 4500 for all models; all other parameters remain constant. The directions of the initial principal stress axes are shown. The pattern in (e) corresponds to the model in Figure 6f. The lateral boundaries have been clipped away in these images to remove the boundary effect.

As such simple domes have radial symmetry in plan view, remote anisotropic tectonic stresses have not had a significant impact on their development; they are therefore thought to have formed during phases of active diapirism due to upwards forces developed by salt at elevated pressure (Withjack & Scheiner 1982; Yin & Grospong 2007).

The geometry of an ideal salt dome can be calculated analytically using the theory of elastic plates (Timoshenko & Woinowsky Krieger 1959). We consider the sediments as a stack of elastic horizontal sheets separated by frictionless interfaces that are bent by a uniform force from underneath generated by fluid (salt) pressure. This is equivalent to the 3D model of laccolithic intrusions developed by Pollard & Johnson (1973). Consider that the salt body is circular in plan view with a radius  $a$ . The distance along the radius is given by  $x$ . The vertical deflection  $w$  of the plates is then given by:

$$w = \frac{P}{64R_e}(a^4 - 2a^2x^2 + x^4) \quad (1)$$

where  $P$  is the driving pressure, which is the difference between the salt pressure and the overburden pressure, and  $R_e$  is the flexural rigidity. The term  $P/R_e$  is unknown, but Equation (1) can be used to establish the normalized profile of an ideal salt dome according to

$$w_n = (1 - 2x_n^2 + x_n^4), \quad (2)$$

where  $w_n$  is the normalized deflection and  $x_n$  is the normalized distance along the radius.

The stress field is calculated using surface curvature and assigned to the triangulated mesh. There are various published methods for using surface curvature to predict fracturing (e.g. Stewart & Podolski 1998; Bergbauer & Pollard 2003). However, many of these methods use *ad hoc* relationships between curvature parameters and fracturing. We use a method in which the bending of rock strata is approximated using the elastic theory of thin plates. According to this theory, when an elastic

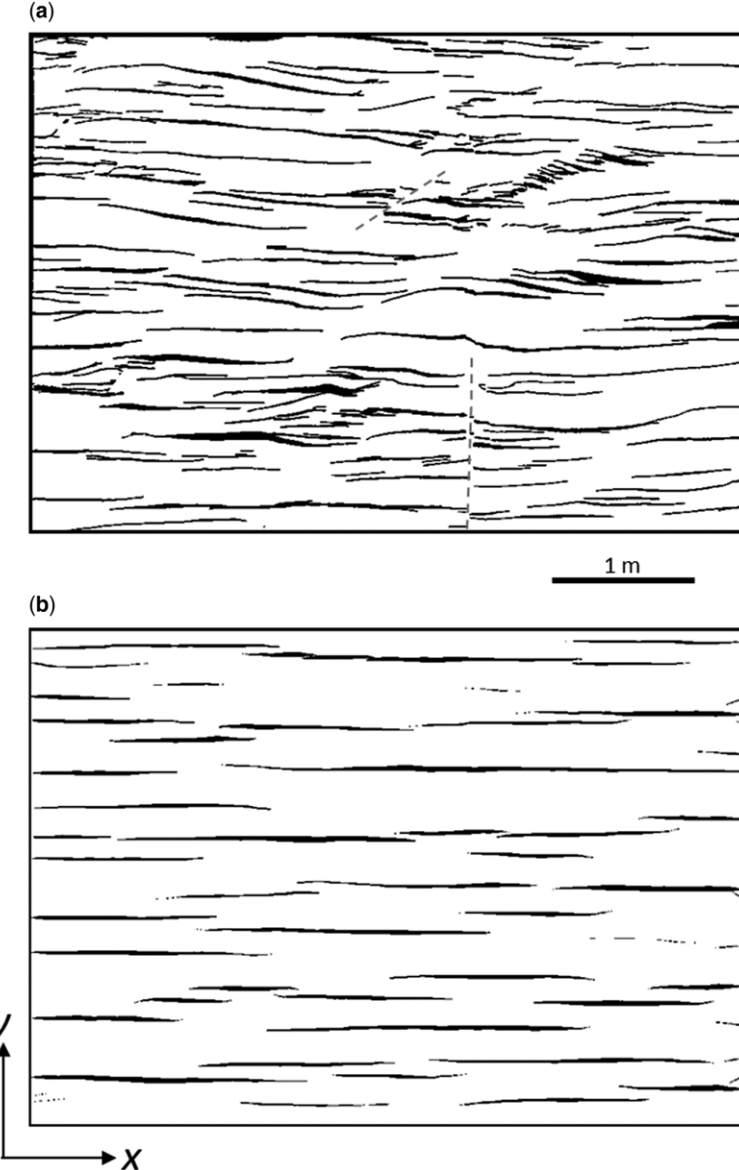


**Fig. 8.** (a) Mapped quartz/siderite veins in the top of an overturned greywacke unit from Millook Haven, Cornwall, UK. Grey dashed lines are zones of shear/pressure solution. (b) Simulation using SCS, with  $S_1$  parallel to y axis. No removal of boundaries was applied.

plate is bent there is an exact relationship between the principal curvatures at any point on the plate and the principal stresses tangential to the surface. The principal stress magnitudes are defined by (Timoshenko & Woinowsky Krieger 1959):

$$S_1 = \frac{Ez}{1 - \nu^2} (k_1 + \nu k_2) \quad (3)$$

$$S_2 = \frac{Ez}{1 - \nu^2} (k_2 + \nu k_1) \quad (4)$$

where  $k_1$  and  $k_2$  are the maximum and minimum curvatures, respectively,  $E$  is Young's modulus,  $\nu$  is Poisson's ratio and  $z$  is the distance above the neutral surface. In the Surface Crack Simulator the

## SUBSEISMIC JOINT AND FAULT NETWORKS SIMULATION

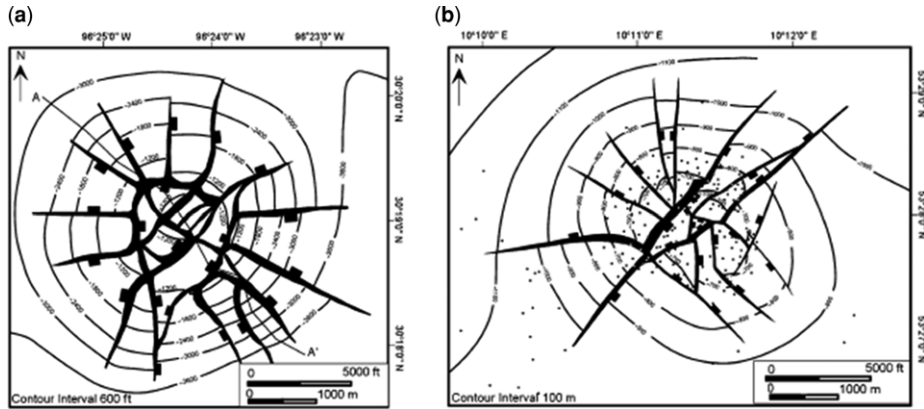


**Fig. 9.** Published examples of fault patterns in salt domes: (a) Clay Creek Dome, Top Wilcox, Gulf of Mexico (after Parker & McDowell 1955); and (b) Reitbrook Dome, Base Tertiary, Germany (after Schmitz & Flixeder 1993). The structural interpretation in both examples is supported by dense borehole data.

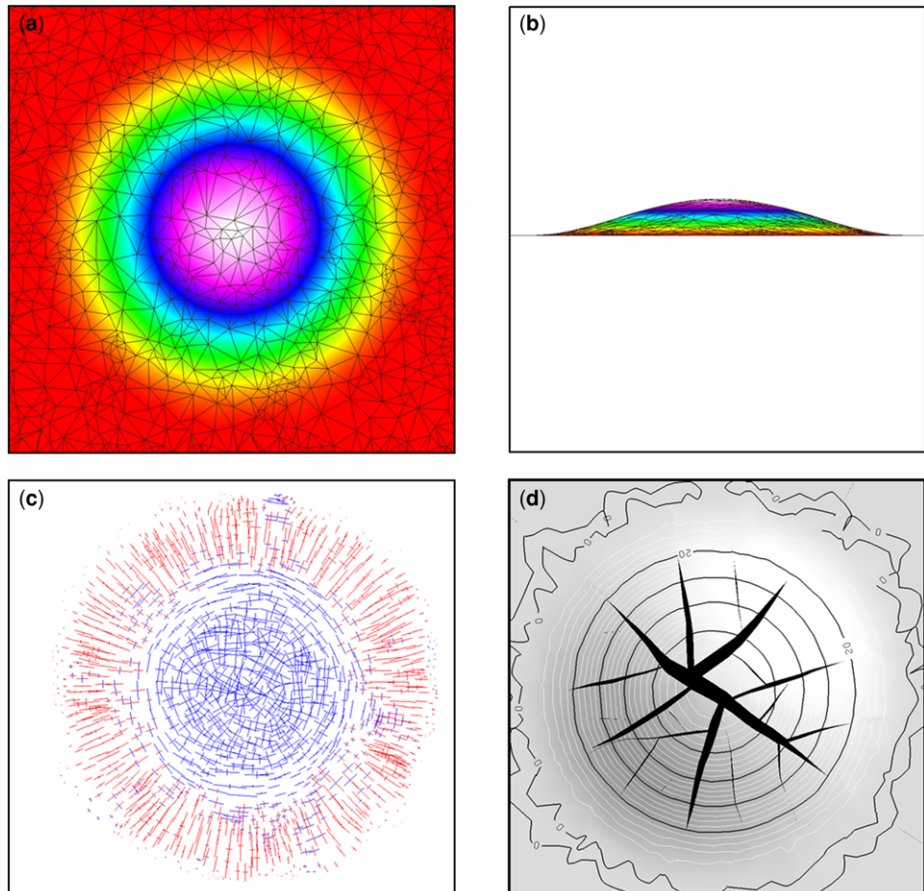


**Fig. 10.** (a) Mesh built from analytical dome model; (b) side view of the dome; (c) stress derived from curvature of the meshed surface (blue, tensile, red compressive); and (d) resulting fault simulation in SCS.

absolute magnitude of the stress tensor is immaterial to the fracture propagation, so we are only concerned with the proportionalities:

$$S_1 \propto (k_1 + \nu k_2) \quad (5)$$

and

$$S_2 \propto (k_2 + \nu k_1). \quad (6)$$

In order to calculate the curvature of the mesh, we use a robust 3D curvature tensor estimation described by Alliez *et al.* (2003). This method estimates the principal curvature vectors accurately for triangular meshes and, unlike methods based on change in surface dip, is accurate even for steep and overturned surfaces. The curvature is measured within a sphere with a user defined averaging radius which determines the length scale of the curvature measurement. The curvature is calculated for the centre of each triangle in the mesh.

In order to create a surface crack simulation, a dome was modelled with a radius of 2000 m and an amplitude of 100 m, and a randomized triangulated mesh was generated to represent the bedding surface (Fig. 10a, b). The stress field on the surface was generated from the principal curvatures using Equations (5) and (6), and Poisson's ratio was set to 0.25 (Fig. 10c).

At the crest of the dome, the stress state is isotropic and tensile: on the flanks of the dome  $S_1$  is tangential, that is, parallel to the structural contours.

Cracks (representing faults) were then grown in the surface to relieve the stress caused by doming. The cracks firstly develop radially and concentric cracks form at later stages, causing the compartmentalization of the structure. The crack width is taken to represent fault heave. The absolute magnitude of the heave is not given by the simulation, but was adjusted heuristically.

Comparison between the SCS results (Fig. 10d) and the natural examples (Fig. 9) indicates that SCS is able to reproduce the main characteristics of the fault pattern. This indicates that the method of using the surface curvature to generate the initial stress condition is successful and also supports the use of the surface cracks to approximate fault patterns. Close examination shows that the heaves of intersecting faults do in some cases decrease towards the branch point. This decrease in heave is not typical of natural fault systems, which have heaves that tend to increase towards the branch points (cf. Fig. 9). A possible explanation is that in natural fault systems a splay may branch from an existing fault, whereas in the simulation the faults nucleate away from existing faults and grow towards them.

## Discussion

The Surface Crack Simulator represents an effective means to simulate joint and fault patterns on bedding surfaces. The resulting fracture patterns have a greater degree of realism than is available in existing mechanical or stochastic methods, and give an improved representation of the network topology. The simulations thereby give an improved basis for flow simulations of fractured and faulted reservoirs.

The input mesh does not put a significant limitation on the kind of fracture pattern that can be generated. However, in order to obtain a high fracture density it is necessary that the mesh is fine. SCS can simulate a range of common fracture patterns, including patterns typical of stratabound joints and faults. Strongly clustered fractures are not easily simulated using this method, however.

As some of the simulation parameters are non physical, they cannot be measured in the laboratory and therefore need to be chosen with heuristically. Well data can provide information about fracture density and orientation, which can be used to calibrate the simulations. Suitable outcrop analogues can also provide additional calibration for the simulations.

The use of horizon curvature to generate the initial stress field in the example of the salt domes opens up the possibility of using the actual curvature of interpreted horizons to generate the initial stress field. This may be valid in areas where buckling or bending stress dominates the regional tectonic stress. Clearly, the technique would not be appropriate where the surface geometry is related to other processes such as deposition and erosion.

In reservoirs with a complex tectonic history, it may be necessary to first create a detailed geomechanical model using a boundary element or finite element solution and use the output stress field to initialize the stress field for SCS. As always with geomechanical modelling, the quality of the results relies on the quality of the understanding of the history and processes of deformation.

The application of the SCS model to faults creates plausible fault patterns. However, the faults occur in the surface only and the vertical offset of the horizon by the faults is not modelled. The fault planes and the vertical offsets have to be included later, as post processing steps. In creating the throws, a decision must be made about which side of the fault is the downthrown side, as this is not specified by the model. In some cases, geological knowledge can be used to assign the down thrown side. For instance, in salt domes it is usual for concentric faults to throw downwards towards the crest of the dome (e.g. Yin & Groshong 2007). In other cases the down thrown side must be

assigned at random. The absolute size of the throw is also not constrained by the simulation; this needs to be constrained by estimates of the total fault strain in the structure.

## Conclusions

The SCS simulations produce realistic simulations of joint patterns that give a good representation of the fracture network geometry and topology. A range of common joint patterns can be developed by varying the stress anisotropy. The joint patterns develop within a single event as the result of stress relief and interaction between the fractures. The aperture of the growing fractures can also be represented in the fracture simulation, and comparison with a naturally occurring vein system is favourable.

To a first approximation we can also use SCS to represent normal fault networks in bedding surfaces, although the vertical offset of the horizons has to be included as a post processing step. By using the curvature to initialize the stress field we can also develop fault/fracture systems related to folding. While these techniques do not intend to rival full geomechanical models, they do represent an advance in our ability to model natural sub seismic fracture systems for inclusion into flow simulations. In the case of fractured reservoirs, the resulting fractures can be brought into discrete fracture network modelling models in which the fractures are represented as surfaces and the details of fluid transport within the fracture system can be simulated. Alternatively, in the case of porous sandstone reservoirs, the modelled faults may be used to ascertain the potential for compartmentalization of the reservoir by sealing faults.

Thanks are due to Sergey Alyaev and John Ivar Haugland for work on developing the code and to David Hunt and Aart Jan van Wijngaarden for their support of this project within Statoil. Thanks also to Tom Manzocchi and an anonymous reviewer for their thorough and helpful reviews.

## References

- ALLIEZ, P., COHEN STEINER, D., DEVILLERS, O., LEVY, B. & DESBRUN, M. 2003. Anisotropic polygonal remeshing. *ACM Transactions on Graphics, Association for Computing Machinery*, **22**, 485–493.
- BAI, T. & POLLARD, D.D. 2000. Fracture spacing in layered rocks: a new explanation based on the stress transition. *Journal of Structural Geology*, **22**, 43–57.
- BARR, D., SAVORY, K.E., FOWLER, S.R., ARMAN, K. & McGARRITY, J.P. 2007. Pre development fracture modelling in the Clair field, west of Shetland. In: LONERGAN, L., JOLLY, R.J.H., RAWNSLEY, K. & SANDERSON, D.J. (eds) *Fractured Reservoirs*. Geological Society, London, Special Publications, **270**, 205–225, <https://doi.org/10.1144/GSL.SP.2007.270.01.14>
- BERGBAUER, S. & POLLARD, D.D. 2003. How to calculate normal curvatures of sampled geological surfaces. *Journal of Structural Geology*, **25**, 277–289.
- BOURNE, S.J. & WILLEMESE, E.J.M. 2001. Elastic stress control on the pattern of tensile fracturing around a small fault network at Nash Point, UK. *Journal of Structural Geology*, **23**, 1753–1770.
- IBEN, H.N. 2007. *Generating surface crack patterns*. PhD thesis, Electrical Engineering and Computer Sciences University of California at Berkeley.
- IBEN, H.N. & O'BRIEN, J.F. 2009. Generating surface crack patterns. *Graphical Models*, **71**, 198–208.
- JACKSON, R.R. 1991. Vein arrays and their relationship to transpression during fold development in the Culm Basin, central south west England. *Proceedings of the Ussher Society*, **7**, 356–362.
- JOHNSTON, D., MCCAFFREY, K., LORIGA, M.A., WATTERSON, J., WALSH, J.J. & GILLESPIE, P.A. 1994. *A Manual Describing Recording, Analysis and Prediction of Vein and Related Fracture Distributions*. MIRO, Lichfield, ISBN: 1 872440 11 8.
- MAERTEN, L., GILLESPIE, P. & DANIEL, J.M. 2006. 3D geomechanical modeling for constraint of subseismic fault simulation. *AAPG Bulletin*, **90**, 1337–1358.
- MANZOCCHI, T. 2002. The connectivity of two dimensional networks of spatially correlated fractures. *Water Resources Research*, **38**, 1–1.
- MATTOS, N.H., ALVES, T.M. & OMOSANYA, K.O. 2016. Crestal fault geometries reveal late halokinesis and collapse of the Samson Dome, Northern Norway: implications for petroleum systems in the Barents Sea. *Tectonophysics*, <https://doi.org/10.1016/j.tecto.2016.04.043>
- MORRIS, J.P., RUBIN, M.B., BLOCK, G.I. & BONNER, M.P. 2006. Simulations of fracture and fragmentation of geologic materials using combined FEM/DEM analysis. *International Journal of Impact Engineering*, **33**, 463–473.
- O'BRIEN, J.F. & HODGINS, J.K. 1999. Graphical modeling and animation of brittle fracture. In *Proceedings of ACM SIGGRAPH 1999*, August, 1999, Los Angeles, California, ACM Press/Addison Wesley Publishing Co., 137–146.
- ODLING, N.E. & WEBMAN, I. 1991. A ‘conductance’ mesh approach to the permeability of natural and simulated fracture patterns. *Water Resources Research*, **27**, 2633–2643.
- OLSON, J.E. 1993. Joint pattern development: effects of subcritical crack growth and mechanical crack interaction. *Journal of Geophysical Research*, **98**, 12,251–12,265.
- OLSON, J.E. & POLLARD, D.D. 1991. The initiation and growth of en echelon veins. *Journal of Structural Geology*, **13**, 595–608.
- OLSON, J.E., LAUBACH, S. & LANDER, R. 2007. Combining diagenesis and mechanics to quantify fracture aperture distributions and fracture pattern permeability. In: LONERGAN, L., JOLLY, R.J.H. & SANDERSON, D. (eds) *Fractured Reservoirs*. Geological Society, London, Special Publications, **270**, 101–116, <https://doi.org/10.1144/GSL.SP.2007.270.01.08>
- PARKER, T.J. & McDOWELL, A.N. 1955. Model studies of salt dome tectonics. *AAPG Bulletin*, **39**, 2384–2470.

- POLLARD, D.D. & AYDIN, A.A. 1988. Progress in understanding jointing over the past century. *Geological Society of America Bulletin*, **100**, 1181–1204.
- POLLARD, D.D. & JOHNSON, A.M. 1973. Mechanics of growth of some laccolithic intrusions in the Henry Mountains, Utah. II. Bending and failure of overburden layers and sill formation. *Tectonophysics*, **18**, 311–354.
- POLLARD, D.D. & SEGALL, P. 1987. Theoretical displacement and stresses near fractures in rock: with application to faults, joints, veins, dikes, and solution surfaces. In: ATKINSON, B.K. (ed.) *Fracture Mechanics of Rock*. Academic Press, Inc., London, 277–349.
- RANK FRIEND, M. & ELDERS, C.F. 2004. The evolution and growth of central graben salt structures, Salt Dome Province, Danish North Sea. In: DAVIES, R.J., CARTWRIGHT, J.A., STEWART, S.A., LAPPIN, M. & UNDERHILL, J.R. (eds) *3D Seismic Technology: Application to the Exploration of Sedimentary Basins*. Geological Society, London, Memoirs, **29**, 149–164, <https://doi.org/10.1144/GSL.MEM.2004.029.01.15>
- RAWNSLEY, K.D., PEACOCK, D.C.P., RIVES, T. & PETIT, J.P. 1998. Jointing in the Mesozoic sediments around the Bristol Channel Basin. *Journal of Structural Geology*, **20**, 1641–1661.
- RENSHAW, C.E. & POLLARD, D.D. 1994. Numerical simulation of fracture set formation: a fracture mechanics model consistent with experimental observations. *Journal of Geophysical Research: Solid Earth* (1978–2012), **99**, 9359–9372.
- RIVES, T., RAZACK, M., PETIT, J. P. & RAWNSLEY, K.D. 1992. Joint spacing: analogue and numerical simulations. *Journal of Structural Geology*, **14**, 925–937.
- RIVES, T., RAWNSLEY, K.D. & PETIT, J.P. 1994. Analogue simulation of natural orthogonal joint set formation in brittle varnish. *Journal of Structural Geology*, **16**, 419–429.
- ROGERS, S., ENACHESCU, C., TRICE, R. & BUER, K. 2007. Integrating discrete fracture network models and pressure transient data for testing conceptual fracture models of the Valhall chalk reservoir, Norwegian North Sea. In: LONERGAN, L., JOLLY, R.J.H. & SANDERSON, D. (eds) *Fractured Reservoirs*. Geological Society, London, Special Publications, **270**, 193–204, <https://doi.org/10.1144/GSL.SP.2007.270.01.13>
- SCHMITZ, J. & FLIXEDER, F. 1993. Structure of a classic chalk oil field and production enhancement by horizontal drilling, Reitbrook, NW Germany. In: SPENCER, A.M. (ed.) *Generation, Accumulation and Production of Europe's Hydrocarbons III*. European Association of Petroleum Geoscientists, Special Publications, Springer Verlag, Berlin, Heidelberg, **3**, 144–154.
- STEWART, S.A. & PODOLSKI, R. 1998. Curvature analysis of gridded geological surfaces. In: COWARD, M.P., DALTABAN, T.S. & JOHNSON, H. (eds) *Structural Geology in Reservoir Characterization*. Geological Society, London, Special Publications, **127**, 133–147, <https://doi.org/10.1144/GSL.SP.1998.127.01.11>
- TIMOSHENKO, S. & WOINOWSKY KRIEGER, S. 1959. *Theory of Plates and Shells*. McGraw Hill, New York, **2**.
- TRIVINO, L.F. & MOHANTY, B. 2015. Assessment of crack initiation and propagation in rock from explosion induced stress waves and gas expansion by cross hole seismometry and FEM DEM method. *International Journal of Rock Mechanics and Mining Sciences*, **77**, 287–299.
- TUCKWELL, G.W., LONERGAN, L. & JOLLY, R.J.H. 2003. The control of stress history and flaw distribution on the evolution of polygonal fracture networks. *Journal of Structural Geology*, **25**, 1241–1250.
- WITHJACK, M. & SCHEINER, C. 1982. Fault patterns associated with domes: an experimental and analytical study. *AAPG Bulletin*, **66**, 302–316.
- YAMADA, Y., OKAMURA, H., TAMURA, Y. & TSUNEYAMA, F. 2005. Analog models of faults associated with salt doming and wrenching: application to offshore United Arab Emirates. In: SORKHABI, R. & TSUJI, Y. (eds) *Faults, Fluid Flow, and Petroleum Traps*. AAPG, Boulder, Memoirs, **85**, 95–106.
- YIN, H. & GROSCHONG, R.H., JR. 2007. A three dimensional kinematic model for the deformation above an active diapir. *AAPG Bulletin*, **91**, 343–363.